# Magic-Size Equilibrium Shapes of Nanoscale Pb Inclusions in Al

U. Dahmen,[1] SQ. Xiao,[1,*] S. Paciornik,[2] E. Johnson,[3] and A. Johansen[3]
[1]*National Center for Electron Microscopy, LBNL, Berkeley, California*
[2]*DCMM PUC-Rio, P.O. Box 38008, Rio de Janeiro, RJ 22463, Brazil*
[3]*Ørsted Laboratory, Niels Bohr Institute, University of Copenhagen, Copenhagen, Denmark*
(Received 9 September 1996)

We show that the equilibrium shapes of small solid Pb inclusions embedded in an Al matrix are size dependent. Using high resolution electron microscopy we have observed that small inclusions a few nanometers in size adopt equilibrium shapes with smooth {111} facets. Inclusion dimensions follow preferred sizes shown to result from the nature of the residual strain which oscillates and decreases with size. As a result, the inclusion shape is controlled by the residual strain energy at small sizes and by the interface energy at larger sizes. [S0031-9007(96)02104-7]

PACS numbers: 61.46.+w, 61.16.–d, 68.55.Jk, 81.10.Aj

One of the most active areas of materials research is the behavior of solids in the nanometer size regime, as their dimensions approach the atomic scale. Electronic, optical, magnetic, mechanical, or thermodynamic properties all may depend on the size and shape of the solid. For example, melting point depressions by several hundred K have been observed for nanosized particles of metals and semiconductors [1–3], whereas large increases in the melting point have been reported for small solid inclusions, i.e., solid particles embedded within another solid [4,5]. The reduction in grain size is also responsible for the unusual properties of nanocrystalline materials [6]. As the dimensions are reduced, shapes and behavior often become discrete, and the existence of magic number sized clusters is now well established for a range of different materials [7]. The diffusion of clusters on a substrate has recently been predicted to depend on magic cluster sizes [8], and quantized or magic sizes also play a special role in the folding of polymer chains [9]. In solid inclusions, preferred sizes were observed in the thickening of plate-shaped $\theta'$ precipitates in Al-Cu alloys [10]. In thin film growth, it has been shown that the shape (though not the size) of small Ag islands on a substrate during growth from the vapor is size dependent and oscillates between a fully faceted and a partially rounded shape [11].

For a crystal in equilibrium with its vapor the Gibbs-Wulff shape minimizes its surface energy for a fixed volume, independent of size [12]. By comparison, a crystal that is embedded in a solid is subject to additional elastic constraints, and at equilibrium it adopts a shape that minimizes the sum of the interface and elastic strain energies:

$$E = E_{\text{int}} + E_{\text{el}} . \quad (1)$$

As a result, the optimum shape of a solid inclusion becomes a function of size. Since the interface energy $E_{\text{int}}$ scales with $r^2$ while the elastic energy scales with $r^3$, the elastic energy will dominate the shape at large sizes, while the interface energy dominates at small sizes. For the isotropic case, inclusions below a critical size will be spherical to minimize the interface energy, while inclusions above the critical size will be plate shaped to minimize the elastic strain energy. Although detailed theoretical treatments of this effect have been given [13], to date, corresponding systematic experimental observations have not been reported.

In the present study we investigate the shapes of nanosized Pb inclusions embedded in an Al matrix. We find that the equilibrium inclusion dimensions tend to take on preferred values dictated by minimum residual mismatch. This often leads to a lowering of the joint symmetry and the creation of asymmetrical shapes which can deviate substantially from the cuboctahedral equilibrium shape of larger inclusions. These observations can be explained as a result of the oscillatory nature of the residual strain energy.

Nanosized Pb inclusions were produced by ion implantation of Pb into 100 nm thick Al films. The films were grown by vapor deposition on single crystal Si substrates at 280 °C and subsequently implanted from the Al surface with 60 keV Pb ions to an average concentration of about 1 at. % at temperatures of 150 °C and 250 °C. The films were back thinned from the Si side to electron transparency and examined by high resolution electron microscopy. To determine the optimum visibility conditions as a function of defocus, foil thickness, inclusion size, and position within the foil, extensive image simulations were carried out [14]. Under optimum conditions, the inclusion dimensions between pairs of edge-on {111} facets could be measured with an accuracy of $\pm 1$ lattice spacing.

The inclusions always adopted a parallel-cube orientation relationship with the matrix and were found to be free of defects [15]. Despite a large difference in lattice parameter, no elastic distortions could be detected around the inclusions using two-beam dynamical imaging conditions which probe the lattice distortion field with high sensitivity [16]. The equilibrium shape, established by electron microscopy observations on large inclusions, equilibrated by melting and resolidification was that of a cuboctahedron,

  

i.e., a regular octahedron bounded by eight {111} faces and truncated on the six {100} faces. Measurements on a significant number of particles showed a ratio of interface energies $\sigma 100/\sigma 111 = 1.15$ [17]. For the smaller particles in the present study, less symmetrical shapes with aspect ratios of up to $1.28 \pm 0.12$ were found [18,19]. The characteristic features are illustrated in Fig. 1(a) which shows a high resolution electron micrograph of a typical region containing several Pb inclusions in the size range of 2 to 10 nm. The crystal lattice is viewed close to a ⟨110⟩ direction where the separation between close-packed atomic planes is 0.23 nm for the Al matrix and 0.29 nm for the Pb inclusions. Because the inclusions are fully embedded within the Al matrix, the overlap of the two lattices gives rise to a moiré contrast effect. The inclusions are seen to vary in size and shape, occasionally showing asymmetrical truncations on {100} planes (see inclusions marked *A*) and often with a different extent of the {111} facets (see inclusions marked *B*). The same asymmetrical shape was often observed to be reestablished after *in situ* melting and resolidification. Unlike the cuboctahedral shape of larger particles, the equilibrium shapes of these small inclusions thus include irregular polyhedra, mainly bounded by eight {111} and to a lesser extent by some (though often not all six) {100} facets. In a ⟨110⟩ projection such as the micrographs shown in Fig. 1 the inclusions display four of the eight {111} facets in edge-on orientation. To characterize the inclusion size accurately, dimensions were measured separately as the distance between opposite pairs of {111} facets, as illustrated for the inclusion shown at higher magnification in Fig. 1(b).

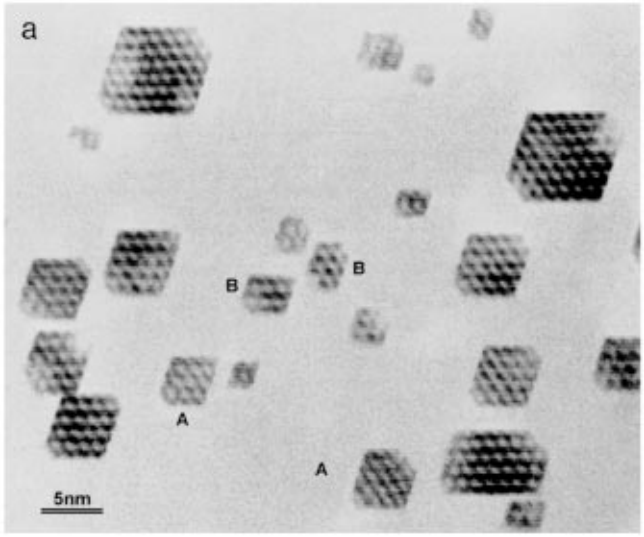


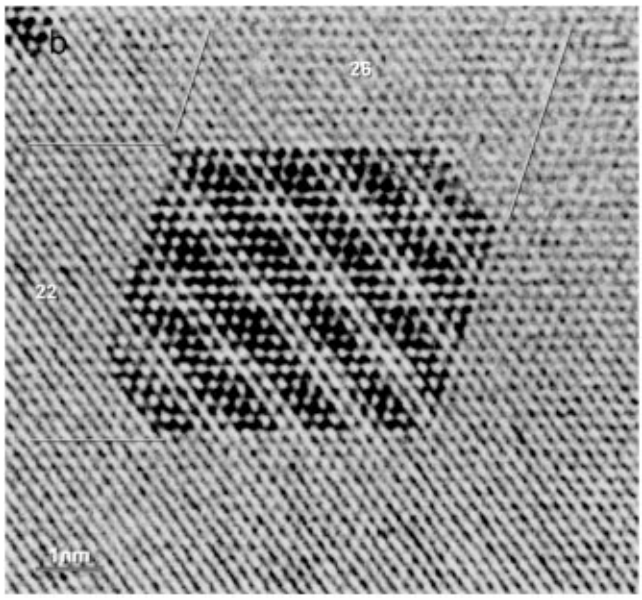


FIG. 1. High resolution electron micrographs in ⟨110⟩ projection showing inclusion shapes and preferred sizes in an Al-Pb alloy after equilibrating the ion-implanted material at ~600 K for 3 h. Inclusion contrast in (a) is due mainly to the moiré effect from overlapping Pb and Al lattices. In (b), a small inclusion is shown at a higher magnification to illustrate its asymmetrical size of $22 \times 26$ Al lattice planes.

Size measurements from a number of high resolution images are plotted as a histogram in Fig. 2. Although its envelope is similar to the Lifshitz-Slyosov-Wagner distribution typical for inclusions in the process of coarsening [20,21], this histogram exhibits oscillatory behavior with periodic minima or gaps at certain sizes. This surprising observation leads to the conclusion that certain inclusion dimensions are unfavorable whereas other are preferred. As shown below, this "quantization" can be understood as a result of the strain energy minimization.

The inhomogeneous elastic strain energy $E_{el}$ of a spherical inclusion under a uniform strain $\varepsilon$ is proportional to $\varepsilon^2$ [22,23]:

$$E_{el} = VA\varepsilon^2. \tag{2}$$

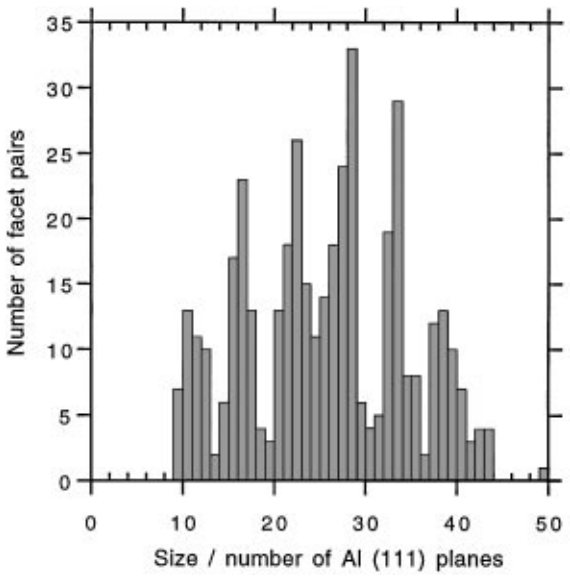


FIG. 2. Histogram of preferred inclusion dimensions (in units of {111} Al plane spacings) measured from high resolution electron micrographs.

Here $A = (18\mu K)/(4\mu + 3K)$ and $\mu$ is the shear modulus of the matrix, $K$ the bulk modulus, and $V$ the volume of the inclusion. The strain $\varepsilon$ is determined by the difference $\Delta V$ in atomic volume of the matrix and inclusion phase, and for small strains, $\varepsilon = \Delta V/3V$. Faceted inclusions such as an octahedron or a tetrahedron have a somewhat lower strain energy, still mainly proportional to $\varepsilon^2$, but modified by logarithmic terms due to elastic relaxation at the sharp edges [24,25].

Pb inclusions in Al are not coherent because the lattice mismatch of 22% is far too large to be accommodated elastically. They are not typically incoherent either because a parallel orientation relationship is strictly maintained [26]. Instead, the large volume change $\Delta V$ is almost entirely accommodated by Al lattice vacancies which are in copious supply near the 600 K melting point of Pb where inclusions are equilibrated (almost $\frac{2}{3}$ of the 933 K melting temperature of Al). However, for a parallel orientation of the lattices and faceted interfaces, vacancies can accommodate the misfit only to the nearest integer number of lattice distances. Therefore, despite the ready supply of vacancies, there remains a *residual* misfit strain

$$\varepsilon_{\text{res}} = \frac{1}{r}\,\Omega(r)\,, \tag{3}$$

where $\Omega(r) = \min_p |qd_{\text{Pb}} - pd_{\text{Al}}|$ is an oscillatory function of the particle size $r = \frac{1}{2}\,pd_{\text{Al}}$ and describes the smallest difference between two corresponding lattice distances $qd_{\text{Pb}}$ and $pd_{\text{Al}}$; $p$ and $q$ are integers. $\Omega$ varies from 0 to half a lattice spacing of Pb, $d_{\text{Pd}}/2$. Substituting in Eq. (2), we obtain the residual strain energy

$$E_{\text{res}} = VA\varepsilon_{\text{res}}^2 = VA\,\frac{\Omega^2(r)}{r^2}\,. \tag{4}$$

Approximating the octahedral shape by a spherical inclusion and with isotropic interfacial energy $\sigma$, Eq. (1) can be written explicitly as

$$E = 4\pi r^2\sigma + \frac{4\pi}{3}\,r\Omega^2(r)\,. \tag{5}$$

The dependence of the inclusion energy on size as given by Eq. (5) is plotted in Fig. 3 for a size range up to 50 lattice planes. Notice the oscillatory behavior showing a nearly periodic variation with size. The solid dots connected by dashed lines indicate that the strain energy is discrete, since an inclusion must contain an integer number of lattice planes. The parabola (dashed line) shows the interface energy. The oscillations of the strain energy term are seen to increase linearly with size. It is apparent that the dominant size regimes for the strain and interface energy terms are the reverse of the usual behavior encountered in the analysis of nucleation and growth: Here the residual strain energy is most important at small sizes whereas the interface energy dominates at larger sizes. For typical values of interfacial and strain energy, the maximum strain energy drops to about 10%

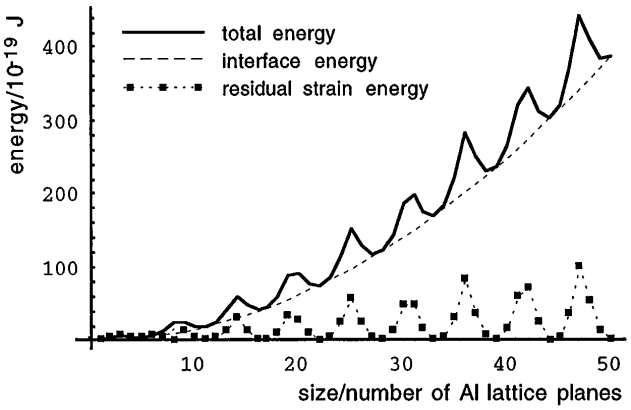


FIG. 3. Plot of inclusion energy [Eq. (5)] as a function of size, showing oscillations due to residual strain energy. The size is given in units of Al plane spacings. (We use an interface energy $\sigma = 90$ mJ/m$^2$, similar to that measured for Ag-Pb [27] and in agreement with Miedema's estimate based the heat of solution [28]. The elastic constants are the shear modulus of Al, $\mu = 28.7$ GPa, and the bulk modulus of Pb, $K = 47.8$ GPa.)

of the interface energy at a size of about 35 nm. Beyond this size, the effect of the residual strain energy on the shape is expected to become small.

A direct comparison of the residual strain energy (dotted line) with the observed histogram of the size distribution is illustrated in Fig. 4. It is clearly apparent that inclusion dimensions tend to cluster around the minima of the oscillating energy function. Inclusions with dimensions of low residual strain are energetically preferred. In the absence of strain energy, an inclusion containing a given number of Pb atoms would tend to form a regular, compact shape (spherical or cuboctahedral). However, if its volume is such that the strain energy of a regular shape is at a maximum, the inclusion can lower its energy by adopting unequal dimensions at neighboring minima. Instead of a regular polyhedron with equal but unfavorable dimensions, an irregular polyhedron with unequal dimensions corresponding to nearby strain energy minima will be preferred. This explains the observation of asymmetric shapes as shown in Fig. 1 and probably accounts for the higher aspect ratios measured for smaller inclusions.

We conclude that small Pb inclusions in Al adopt equilibrium shapes that are faceted, display magic sizes, and can be irregular in shape.

The phenomenon of magic sizes and asymmetries in the equilibrium shape of small inclusions, reported here for the first time, is not expected to be limited to Pb inclusions in Al. Crystalline inclusions in topotaxial alignment with a crystalline matrix are typical for most alloy systems in which precipitates form from a supersaturated solid solution. In many cases, the precipitates nucleate and grow under conditions of high vacancy concentrations similar to those prevalent in the present study. However, even when strain accommodation requires the formation

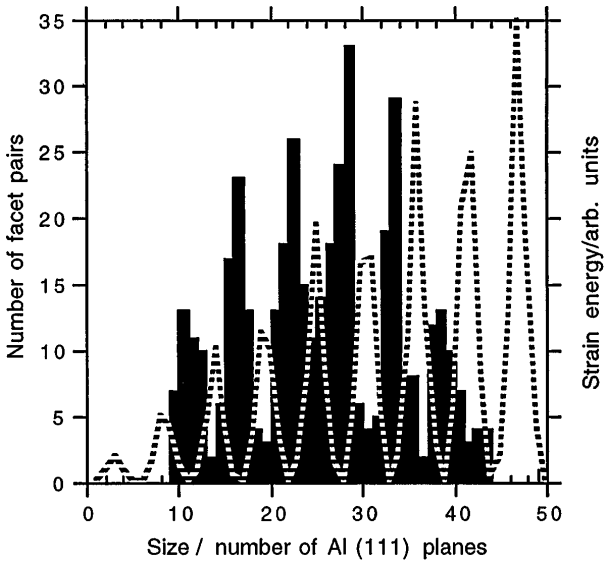


FIG. 4. Comparison of oscillation in observed size distribution (solid histogram) with residual elastic strain energy (dotted line) as a function of size. Gaps in the histogram coincide with peaks in the elastic strain energy. The envelopes of the two plots are unrelated.

of dislocation loops, the discrete nature of the matrix and inclusion lattices leads to an oscillatory behavior of the residual strain energy and corresponding optimum sizes. The observations and analysis presented here thus have broad implications for the nucleation and equilibrium shape of small inclusions and the growth of large inclusions in many alloy systems.

This work is supported by the Director, Office of Energy Research, Office of Basic Energy Sciences, Materials Sciences Division of the U.S. Department of Energy under Contract No. DE-AC03-76SFOOO98, and by the Danish Natural Sciences Research Council. One of us (U. D.) is indebted to the CNRS-CECM for support during a sabbatical leave.

*Present address: Riga Analytical Lab, Inc., 3375 Scott Blvd, Suite 132, Santa Clara, CA 95054.

[1] M. Takagi, J. Phys. Soc. Jpn. **9**, 359 (1954).
[2] A. N. Goldstein, C. J. Echer, and A. P. Alivisatos, Science **256**, 1425 (1992).
[3] P. R. Couchman and W. A. Jesser, Nature (London) **269**, 481 (1977).
[4] H. Saka, Y. Nishikawa, and T. Imura, Philos. Mag. A **57**, 895 (1988).
[5] L. Gråbæk, J. Bohr, H. H. Andersen, A. Johanson, E. Johnson, and I. K. Robinson, Phys. Rev. B **45**, 2628 (1992).
[6] For a review, see H. Gleiter, Prog. Mater. Sci. **33**, 223 (1989).
[7] See, for example, *Clusters of Atoms and Molecules*, edited by H. Haberland (Springer-Verlag, Berlin, 1994).
[8] J. C. Hamilton, Phys. Rev. Lett. **77**, 885 (1996).
[9] P.-A. Lindgård and H. Bohr, Phys. Rev. Lett. **77**, 779 (1996).
[10] W. M. Stobbs and G. R. Purdy, Acta Metall. **26**, 1069 (1978).
[11] J. Tersoff, A. W. Denier van der Gon, and R. M. Tromp, Phys. Rev. Lett. **70**, 1143 (1993).
[12] C. Herring, Phys. Rev. **82**, 87 (1951).
[13] A. G. Khachaturyan, S. V. Semenovskaya, and J. W. Morris, Jr., Acta Metall. **36**, 1563 (1988); M. McCormack and J. W. Morris, Jr., Acta Metall. Mater. **40**, 2489 (1992).
[14] S. Paciornik, S. Q. Xiao, S. Hinderberger, E. Johnson, and U. Dahmen, Proc. MSA **53**, 646, 648 (1995).
[15] H. H. Andersen and E. Johnson, Nucl. Instrum. Methods Phys. Res., Sect. B **106**, 480 (1995).
[16] P. B. Hirsch, A. Howie, R. B. Nicholson, D. W. Pashley, and M. J. Whelan, *Electron Microscopy of Thin Crystals* (Butterworths, London, 1965).
[17] K. L. Moore, D. L. Zhang, and B. Cantor, Acta Metall. Mater. **38**, 1327 (1990).
[18] B. Schmidt, MSc thesis, University of Copenhagen, 1992.
[19] S. Q. Xiao, E. Johnson, S. Hinderberger, A. Johansen, K. K. Bourdelle, and U. Dahmen, J. Microsc. **180**, 61 (1995).
[20] I. M. Lifshitz and V. V. Slyosov, J. Phys. Chem. Solids **19**, 35 (1961).
[21] C. Wagner, Z. Electrochem. **65**, 81 (1961).
[22] J. W. Christian, *The Theory of Phase Transformations in Metals and Alloys* (Pergamon Press, Oxford, 1975).
[23] J. D. Eshelby, Proc. R. Soc. London A **241**, 376 (1957).
[24] R. DeWit, Phys. Status Solidi **20**, 575 (1967).
[25] G. Kalonji and J. W. Cahn, Philos. Mag. A **53**, 521 (1986).
[26] Observations by high resolution electron microscopy show that the interface may not be described as semicoherent either because no signs of localized atomic relaxation into interfacial dislocations were found. Similar "noncoherent" interfaces have been found in weakly bonded systems such as Al on Si [F. K. LeGoues, W. Krakow, and P. S. Ho, Philos. Mag. A **53**, 833–841 (1986)], or Pd on $Al_2O_3$ [T. Muschik and M. Rühle, Philos. Mag. A **65**, 363 (1992)].
[27] J. W. Martin and R. D. Doherty, *Stability of Microstructures in Metallic Systems* (Cambridge University Press, Cambridge, 1976).
[28] A. R. Miedema, Solid State Commun. **39**, 1337 (1981).